Review of
Scientific Instruments

RESEARCH ARTICLE | FEBRUARY 27 2025

Combining an *in situ* device fabrication and six-probe electrical transport measurement system with low-energy electron microscopy

Jin Zhao ; Ivan Bespalov ; Rongting Wu ✉ ; Ivan Božović ✉

Rev. Sci. Instrum. 96, 023907 (2025)
https://doi.org/10.1063/5.0251787

AIP
Publishing

Review of
Scientific Instruments

ARTICLE

pubs.aip.org/aip/rsi

Combining an *in situ* device fabrication and six-probe electrical transport measurement system with low-energy electron microscopy

Cite as: Rev. Sci. Instrum. 96, 023907 (2025); doi: 10.1063/5.0251787
Submitted: 4 December 2024 • Accepted: 31 January 2025 •
Published Online: 27 February 2025

View Online Export Citation CrossMark

Jin Zhao,[1,2,a)] Ivan Bespalov,[1,2,b)] Rongting Wu,[3,4,5,c)] and Ivan Božović[1,2,6,7,c)]

AFFILIATIONS

[1] Energy Sciences Institute, Yale University, West Haven, Connecticut 06516, USA
[2] Department of Chemistry, Yale University, New Haven, Connecticut 06511, USA
[3] Department of Applied Physics, Yale University, New Haven, Connecticut 06511, USA
[4] State Key Laboratory of Semiconductor Physics and Chip Technologies, Institute of Semiconductors, Chinese Academy of Sciences, Beijing 100083, China
[5] Center of Materials Science and Optoelectronics Engineering, University of Chinese Academy of Sciences, Beijing 100049, China
[6] Shanghai Advanced Research in Physical Sciences (SHARPS), Pudong, Shanghai 201203, China
[7] Brookhaven National Laboratory, Upton NY 11973, USA

[a)] **Current address:** Department of Physics, Emory University, Atlanta, Georgia 30322, USA.
[b)] **Current address:** Steele Laboratory, Department of Applied Physics and Materials Science, California Institute of Technology, Pasadena, California 91125, USA.
[c)] **Authors to whom correspondence should be addressed:** rtwu@semi.ac.cn and bozovic.hts@gmail.com

ABSTRACT

Two-dimensional (2D) quantum materials, including several analogs of graphene (“X-enes”), are of great current research interest. However, some of the potentially most exciting ones are reactive and sensitive to exposure to the atmosphere, which hampered the experimental study of their key physical properties. Here, we introduce an experimental setup that integrates sub-atomic-layer-resolved molecular beam epitaxy (MBE) synthesis, real-time low-energy electron microscopy (LEEM) and low-energy electron diffraction (LEED), and *in situ* six-probe electrical transport measurements. The six-probe apparatus is equipped with a dry cryocooler for reaching cryogenic temperatures, a piezoelectric XYZ nano-positioning stage for high-precision motion of the six probes, and an *in situ* device fabrication system for the deposition of custom-shaped gold electrodes. This design enables the six-probe system to perform both AC and DC resistance measurements on 2D quantum materials along multiple orientations within the temperature range of 5K $< T <$ 400 K. The modules are interconnected under ultrahigh vacuum (UHV), and the samples can be synthesized by MBE, imaged by LEEM, and R(T) dependence measured without any surface contamination. We present the first experimental results that test and validate the performance of the six-probe system by transport measurements on several materials, including semiconductors and superconductors. This new instrument is proven to be a versatile platform for studying atmosphere-sensitive quantum materials.

I. INTRODUCTION

Study of the physical properties of two-dimensional (2D) quantum materials is currently one of the most active topics in condensed matter physics research. In part, this interest originates from theoretical predictions of 2D superconductivity.[1,2] One of the candidate 2D superconductors is borophene, which was predicted to reach a critical temperature (T_c) of up to 33 K.[3–7] Despite significant advances in borophene synthesis, ranging from nanometer-scale islands[8] to micrometer-sized sheets that could potentially be used to fabricate borophene-based devices,[9–11] superconductivity in borophene has not yet been experimentally confirmed. One reason is that borophene is unstable under ambient conditions;[12,13] exposure to the atmosphere transforms it into insulating boron oxide.[14] For this reason, the standard *ex-situ* transport measurement techniques that require exposing the sample after synthesis under atmospheric conditions to fabricate the electrodes and then transfer the sample to the transport-measurement setup cannot access the intrinsic physical properties of borophene. This calls for developing an experimental approach enabling well-controlled synthesis, structural and morphological characterization, electrode fabrication, and electrical transport measurements of borophene and other atmosphere-sensitive materials under UHV conditions.

Here, we present an experimental setup that integrates an MBE synthesis chamber, an *in situ* device fabrication system, and a six-probe apparatus (all custom-designed and built), with a low-energy electron microscope (LEEM). LEEM enables monitoring of the morphology and the crystal structure of the film in real-time, from the initial growth stage until the formation of a continuous film with full surface coverage.[15–17] LEEM-guided MBE thus enables well-controlled synthesis of the quantum material of choice. After growth, the R(T) dependence of the film can be measured in the six-probe chamber at both millimeter and micrometer scales using the macro (macro-6PP) and micro (micro-6PP) six-point probe modes,[18] respectively. All these operations can be performed without exposing the sample to the atmosphere, hence preserving the intrinsic material properties throughout the entire research cycle. The combination of MBE–LEEM with the six-probe transport measurements within a single integrated UHV facility enables future research of the electrical transport properties of various atmosphere-sensitive 2D quantum materials.

II. SIX-PROBE SYSTEM

A. System design

Figure 1 depicts the schematic diagram of the MBE/LEEM/six-probe UHV system. The overall base pressure is better than 2×10^{-10} Torr. The system consists of three interconnected UHV chambers: a preparation chamber, a main chamber, and a six-probe transport measurement chamber. The preparation chamber [Fig. 1(a)] hosts equipment for sample cleaning by sputtering, annealing, and fabrication of contact electrodes by evaporating gold through a custom-shaped shadow mask using an effusion cell (K-Cell Evaporator-1, FUTEC Corp). The main chamber [Fig. 1(b)] is equipped with a commercial LEEM/LEED/PEEM system (LEEM III, Elmitec GmbH), an electron-beam evaporator (EFM 3, Focus GmbH), a high-temperature effusion cell (HTEZ, Dr. Eberl MBE-Komponenten), a RF plasma source (HD25, Oxford Applied Research) for supplying atomic hydrogen or nitrogen, and several home-made low-temperature effusion cells. For imaging in photoemission electron microscopy (PEEM) mode, the main chamber is equipped with a Hg arc lamp (Newport Corp). By using different

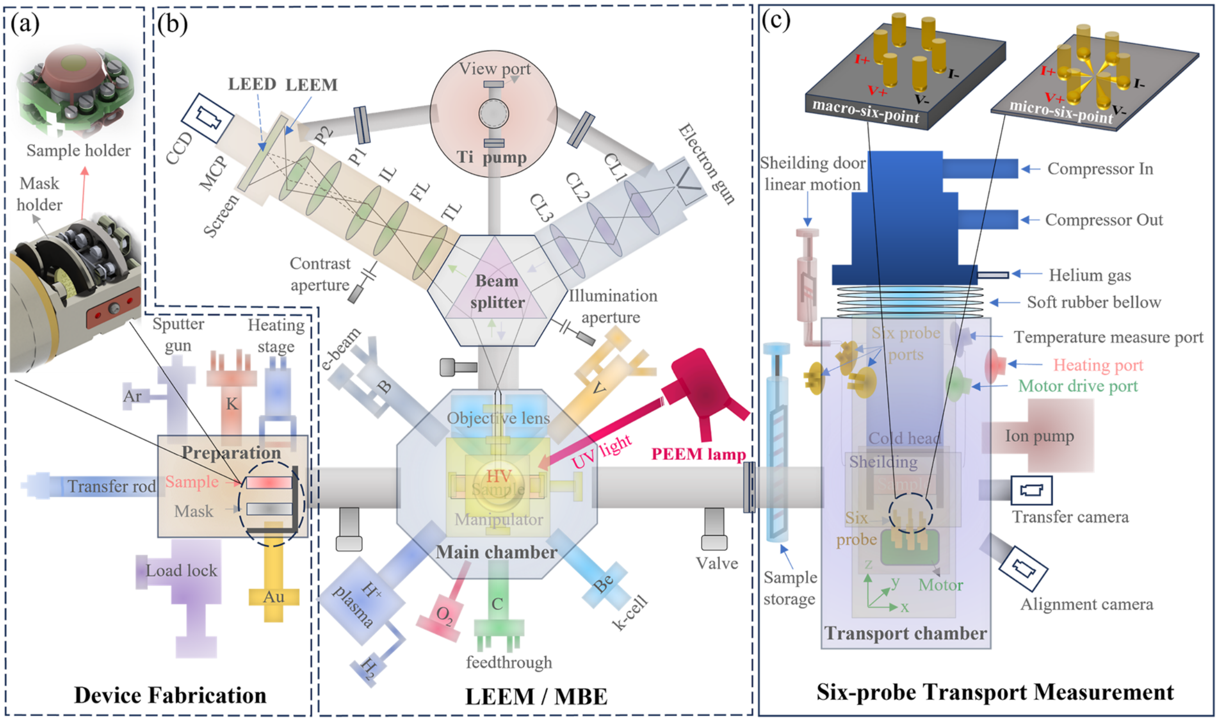

FIG. 1. Schematic diagram of the MBE–LEEM/six-probe system. (a) A preparation chamber containing a setup for sample cleaning by sputtering, annealing, and fabrication of electrodes for six-probe measurements. (b) A main chamber with several MBE sources (electron beam and Knudsen-cell) and a LEEM/LEED/PEEM instrument. (c) A home-made *in situ* six-probe system for electrical transport measurements.

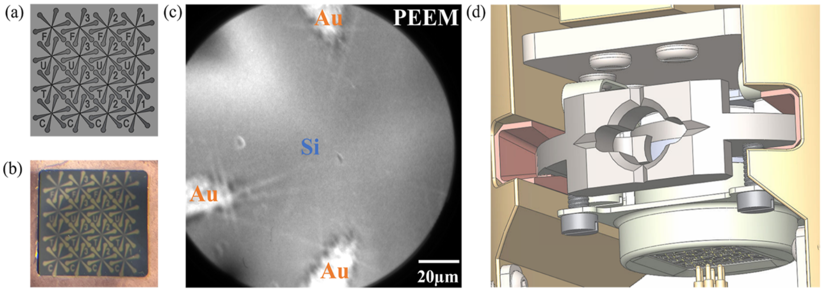

FIG. 2. Micro-6PP electrical transport measurement mode. (a) Mask design pattern for 4 × 4 six-probe devices. Each device is labeled by the combination of a character and a number. (b) The *in situ* grown 4 × 4 six-probe device pattern with gold electrodes deposited at 1000 °C for 3 min on a 10 × 10 mm^2 sample. All electrodes and labels are clearly visible. (c) PEEM image of gold electrodes deposited on a Si(111) wafer. The field of view for the PEEM image is 150 μm. The separation between *in situ* grown electrodes is around 50–60 μm, allowing for micrometer-scale resistance measurement at the center. (d) Sample on the *in situ* transport measurement stage in the transport chamber connected with the LEEM system. The sample with 4 × 4 six-probe device pattern is fixed and faces down. A six-point spring-leg probe on an XYZ nano-positioning stage can navigate and land on the target device on the surface for micrometer-scale resistance measurement.

targets in the MBE sources, various 2D materials can be grown. For example, we use a polycrystalline boron (B) target for the growth of borophene. The electron trajectory and imaging modes (LEEM/LEED) can be adjusted and switched by modifying the current in the lens system.

The home-made *in situ* six-probe electrical transport measurement system is shown in Fig. 1(c). The system utilizes a 1.1-W 4 K dry cryocooler (Advanced Research Systems, Inc.) for reaching cryogenic temperatures. Helium gas serves as the heat exchange medium and is filled in between the cryocooler and sample stage, which are connected by a soft rubber bellow. This design ensures minimization of mechanical vibrations and improves the mechanical stability of the six-probe during the measurements. A six-point spring-leg probe is mounted on a piezoelectric XYZ nano-positioning stage (FUTEC Corp.) with a maximum XYZ directional motion range of 7 × 7 × 10 mm^3. This allows moving the six probes along the sample surface and selecting areas of interest for measurements with the assistance of an alignment camera. The six probes are arranged in a hexagon-like shape, enabling electrical transport measurements along multiple directions. Two cold shields are installed at the 50 K cryostat and the 4 K cryostat to minimize heating by radiation. The shields have two shielding doors that can be moved linearly and controlled simultaneously. The doors are opened when transferring the sample in or out and are closed to achieve the lowest temperature of 5 K. A heater and a silicon diode are installed at the 4 K cryostat, and the temperature control is achieved using a cryogenic temperature controller (Model 335, Lake Shore Cryotronics, Inc). The system has six additional electrodes for direct sample holder heating and on-chip gating, enabling versatile resistance measurements.

B. Six-probe system operation modes

The six probes are arranged in a hexagonal pattern with an equidistant probe spacing of 1.2 mm, supporting two operation modes for sample resistance measurements. The macro-6PP mode millimeter-scale resistance measurements are performed by directly landing the spring-loaded contact legs of the six probes onto the sample surface. In the micro-6PP mode, the legs of the six probes land onto the gold contact pads of a custom-shaped electrode device that is *in situ* fabricated on the sample surface. The electrode spacings can be varied by using different custom-shaped masks and gold evaporation parameters. This mode enables micrometer-scale resistance measurements at the electrode centers.

Figure 2 illustrates the resistance measurement process in the micro-6PP mode. Before the resistance measurements, a custom-shaped electrode pattern mask [Fig. 2(a)] is inserted in the preparation chamber above the effusion cell serving as the gold source. After deposition at the K-cell temperature of 1000 °C for 3 min, the gold electrodes are formed on the sample surface [Si(111) shown here] located above the mask [Fig. 2(b)]. After the electrode deposition, the sample is transferred to the MBE chamber. The sample electrode contacts are inspected in the PEEM mode [at a field of view of 150 μm in Fig. 2(c)] to ensure the proper shape of and separation between the deposited electrodes. In Fig. 2(c), the separation between the *in situ* grown electrodes is 50–60 μm, allowing for micrometer-scale resistance measurement at the center. In addition, for quantum 2D materials grown by MBE, LEEM/PEEM can confirm alignment between the gold electrodes at the selected region of the sample (a 2D material flake, an island, or a single-crystal domain), ensuring that the resistance measurement is made at the desired location. After device fabrication, the sample with the gold electrode pattern is transferred to the six-probe chamber [Fig. 2(d)]. With the assistance of the alignment camera and the custom-shaped labels patterned on the sample [e.g., F1, U1, T1, and C1 in Fig. 2(c)], we can navigate the six probes above the sample surface to find the region of interest and ensure that the six probes are properly contacting the gold electrodes for resistance measurements in the micro-6PP mode.

III. EXPERIMENTAL RESULTS

A. Resistance measurements in macro-6PP and micro-6PP modes

Figure 3 shows the experimental results of macro-6PP and micro-6PP resistance measurement mode on several samples. The

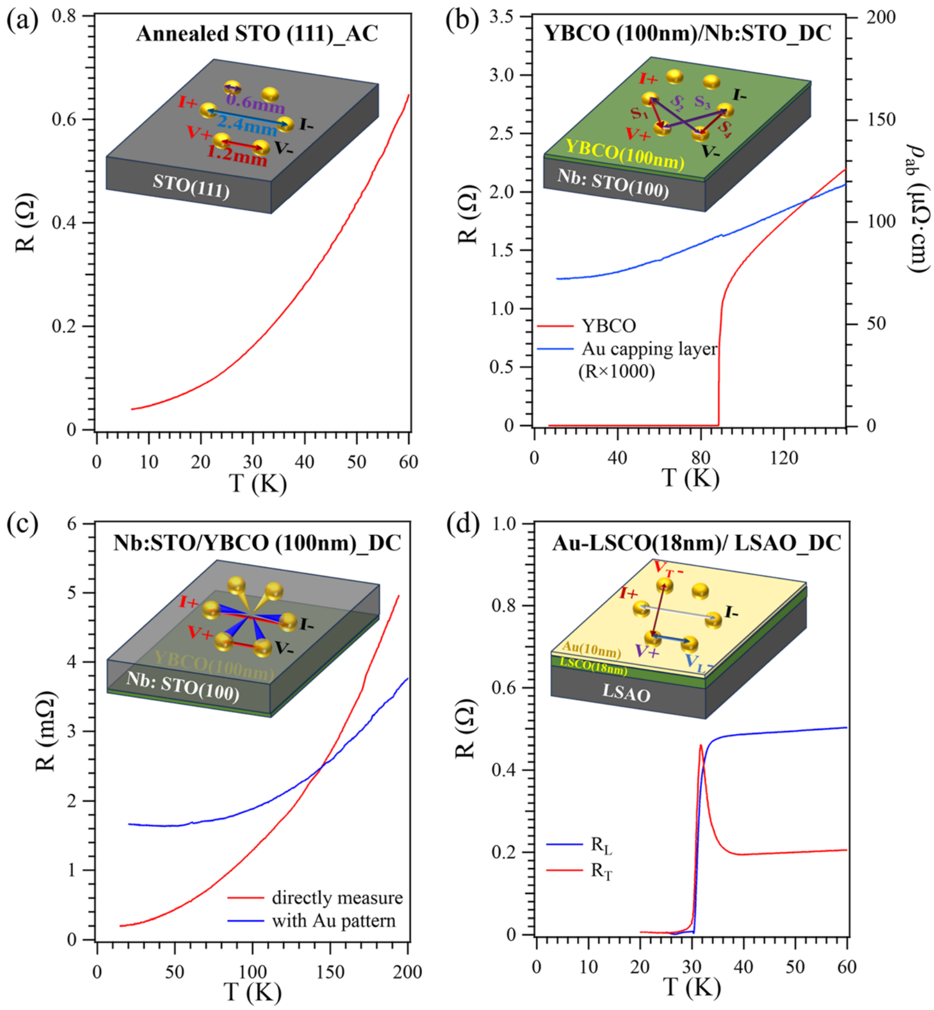

FIG. 3. Macro-6PP and micro-6PP resistance measurement on several samples. (a) The macro-6PP measured the AC resistance curve of STO (111) after *in situ* vacuum annealing at 1000 °C for 2 h in the MBE chamber. The illustration shows the dimensions of the six probes and the wiring configuration for current and voltage measurements. (b) The macro-6PP measured the DC resistance and resistivity curve (red) of the YBCO (100 nm)/0.7 wt. % Nb-doped STO (100) sample. The blue curve is the measured DC resistance curve (the values are multiplied by 1000) after depositing a gold capping layer at 1000 °C for 3 h. (c) Measured DC resistance curve of the backside of YBCO (100 nm)/0.7 wt. % Nb-doped STO (100) sample with (blue curve, micro-6PP) and without (red curve, macro-6PP) device patterning. The gold electrode pattern was created by evaporating at 1000 °C for 3 min. (d) DC resistance curves of LSCO (18 nm)/LSAO with 10 nm gold capping layers measured in the macro-6PP mode. The red curve represents the transverse resistance. The blue curve represents the longitudinal resistance. The wiring configuration for current and voltage measurements is shown in the illustration.

diameter of each probe is 0.6 mm, and the six probes are arranged in a regular hexagonal pattern with a side length of 1.2 mm. The current and voltage are measured using lock-in amplifiers (Model SR830, Stanford Research Systems Inc.) in either AC or DC mode. Different wiring configurations for current and voltage can also be selected according to the needs of the experiment. Figure 3(a) shows the R(T) dependence, measured in the AC macro-6PP mode, of the $SrTiO_3$ substrate (STO, MTI Corp). The STO sample was insulating as received but was rendered conducting by *in situ* annealing in the MBE chamber under high vacuum at 1000 °C for 2 h.

In Fig. 3(b), the red curve shows the R(T) dependence, measured in the DC macro-6PP mode, in an optimally doped $YBa_2Cu_3O_{7-\delta}$ film (YBCO, MTI Corp) grown on a 0.7 wt. % Nb-doped STO(100) substrate. The thickness $t = 100$ nm of this YBCO film is much smaller than the probe spacing $s = 1.2$ mm, so the film can be modeled approximately as an infinte 2D sheet. In this case, when $t << s$, the voltage drop V between the two inner probes[19] is given by

$$V = V_2 - V_3 = \frac{I\rho}{2\pi t} \ln\left(\frac{s_2 s_3}{s_1 s_4}\right). \tag{1}$$

For the special case of the four-point probe geometry shown in Fig. 3(b), with $s_1 = s_4 = s$ and $s_2 = s_3 = \sqrt{3}\, s$, the resistivity of YBCO is given by

$$\rho = \frac{2\pi t}{\ln 3} R, (R = V/I). \tag{2}$$

Some studies[20,21] propose a correlation between probe spacing and the penetration depth of the electrical current into the crystal: increasing the probe spacing should enhance the current penetration depth, making measurements more bulk-sensitive, while decreasing the probe spacing is making measurements more surface-sensitive. To estimate the current penetration depth of our six-probe system in the macro-6PP mode, a gold capping layer was deposited for 3 h on YBCO, with the source temperature kept at 1000 °C. We observed that the measured conductance comes entirely from the gold capping layer (the blue curve), indicating that the current

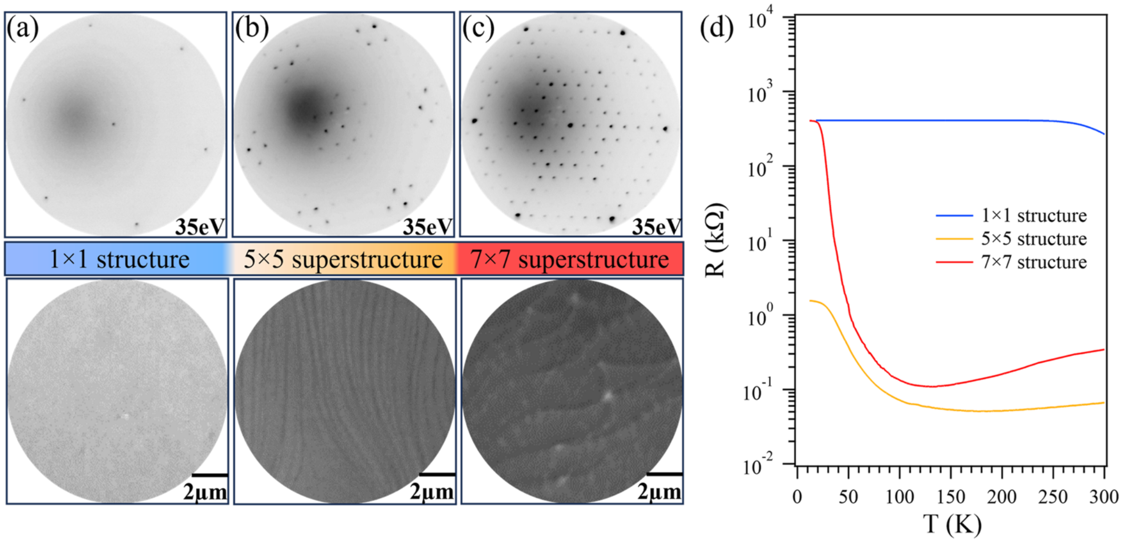

FIG. 4. LEED patterns/LEEM images and transport measurements of n-type undoped Si (111). (a) Si(111) surface with a 1 × 1 structure. (b) Si(111) surface with a 5 × 5 superstructure. (c) Si(111) surface with a 7 × 7 superstructure. All three LEED patterns were taken at 35 eV. The field of view in LEEM images is 40 μm. (d) Measured DC resistance curves of the three Si(111) surfaces.

essentially did not penetrate through the gold capping layer into the superconducting layer. By substituting the measured resistance value and the known resistivity of gold into Eq. (2), we can estimate the current penetration depth to be in the range of several micrometers.

When we placed the six probes on the back (STO) side of the same YBCO/STO sample, we found that the current also did not penetrate through the STO substrate into the superconducting layer [the red curve in Fig. 3(c), macro-6PP]. In general, the sample material, the crystal quality, and interface resistances affect the current penetration depth.

After depositing the gold electrode pattern through the shadow mask for 3 min, with the source kept at 1000 °C, the effective probe spacing decreased from 1.2 mm to around 50 μm. Concomitantly, the measured resistance changed [the blue curve in Fig. 3(c), micro-6PP], showing a smaller resistance at high temperatures and a larger resistance at low temperatures, yielding a smaller residual resistivity ratio (RRR). This indicates that the micro-6PP mode is, indeed, more surface-sensitive than the macro-6PP mode, as predicted, with the resistance measurements being predominantly probed in the surface layer of STO with poorer crystallinity. In addition, there is no big difference in resistances measured by these two modes, which agree with the results reported in the literature.[19]

Figure 3(d) shows the measured longitudinal (blue) and transverse (red) DC resistance curves of the optimally doped $La_{1.84}Sr_{0.16}Cu_2O_4$ film, $t = 18$ nm thick, grown on the $LaSrAlO_4$ (LSAO) substrate with a 10 nm gold capping layer. A significant difference is apparent between the longitudinal and transverse resistances of LSCO, which is consistent with the literature.[22] This is a demonstration that our six-probe system can detect the anisotropy of in-plane resistivity. The spare electrodes can be used for Hall coefficient measurements and *in situ* gating experiments in future experiments.

B. Combining LEEM/LEED with *in situ* transport measurement

Figure 4 shows the LEED patterns, LEEM micrographs, and macro-6PP R(T) curves taken from an *n*-type undoped Si(111) substrate (MTI Corp). All LEED patterns were taken at 35 eV, and the LEEM field of view was 40 μm. The operational sequence is as follows: First, we load the sample and anneal it to achieve the desired surface reconstruction. Second, we measure its LEED patterns and LEEM micrographs. Third, for each surface reconstruction, we transfer the sample to the transport chamber for cryogenic resistance measurements. Finally, we transfer the sample back to the LEEM chamber to revisit its LEED patterns and LEEM images. These three surface reconstructions are relatively stable within the indicated temperature ranges, while showing significantly different resistivities. After the transport measurements using LEED, we confirmed that the structures remained essentially the same, without transitioning from one reconstruction to another. Even after prolonged resistance measurements that involved repeated heating and cooling cycles, which caused surface adsorption of gas that blurred the LEED patterns, after a few subsequent annealing cycles under the indicated reconstruction conditions, we were able to remove the adsorbed gas and restore clear original patterns.

The Si(111) surface with a 1 × 1 structure was obtained by vacuum annealing at 650 °C overnight [Fig. 4(a)]. This 1 × 1 Si(111) exhibits an insulating behavior [the blue curve in Fig. 4(d)]. The nearly temperature-independent resistance at low temperatures may originate from the surface SiO_2 layer. The melting point of the naturally formed SiO_2 layer is much higher than that of Si, and our six-probe system is more sensitive to the surface conductivity. Hence, the presence of the residual SiO_2 layer would naturally be detected. The resistivity of this native oxide layer is relatively low, limiting the further increase in resistance at low temperatures.

Some reports suggested that wide terraces and continuous annealing at relatively higher temperatures are required to achieve pure 5 × 5 surface reconstruction.[23,24] By experimental exploration, a Si(111) surface with a 5 × 5 superstructure was obtained by flash-heating several times to 1200 °C for 10 s and slowly cooling down. The terraced surface is clearly visible in the LEEM image [Fig. 4(b)]. The resistance here exhibits a metallic behavior above 176 K, while at low temperatures, it shows weakly insulating properties [the orange curve in Fig. 4(d)]. Anisotropic resistivities of these and similar terrace structures could be studied in our system in the future, by measuring the R(T) dependence along various directions in the plane.

A Si(111) surface with a 7 × 7 superstructure is one of the most studied silicon surface terminations. Yet, there is still an ongoing debate in both theoretical and experimental reports regarding whether it shows metallic or insulating behavior at different temperatures.[25–30] In our experiments, a clear Si(111) surface with the 7 × 7 superstructure was obtained by flash-heating the Si(111) sample several times in UHV up to 1300 °C for 10 s [Fig. 4(c)]. It shows an evident metal–insulator transition; the resistivity has a metallic behavior above 133 K, while at lower temperatures, it shows strongly insulating properties [the red curve in Fig. 4(d)]. This is consistent with the insulating phase observed in scanning tunneling and photoemission spectroscopy experiments[31] at low temperatures.

IV. CONCLUSION

We have demonstrated successful integration of MBE, LEEM/LEED, and six-probe electrical transport measurement techniques under UHV conditions. The system enables *in situ* electrode device fabrication and cryogenic electrical transport measurements in both macro-6PP and micro-6PP modes. We have demonstrated *in situ* resistance measurements of STO(111), Nb-doped STO(001), YBCO, LSCO, and Si(111). In LSCO, which has anisotropic in-plane resistivity, we measured longitudinal and transverse resistances. In Si(111), we obtained and verified by LEED three different Si(111) surface reconstructions (1 × 1, 5 × 5, and 7 × 7) and performed *in situ* surface resistance measurements on each of them. The Si (111) surface reconstruction with the 7 × 7 superstructure showed a metal–insulator transition at around 133 K.

This is the first time that techniques such as sample synthesis by molecular beam epitaxy, structural characterization by electron microscopy and diffraction, device fabrication, and *in situ* transport measurements have been integrated within one UHV system. This key technical advance enables the study of surface structure and surface transport properties of surface-sensitive quantum materials (such as 2D superconductors and X-enes.), even if these form just micrometer-sized flakes. Moreover, compared to the traditional four-probe setup, the six-probe configuration is better suited for measuring anisotropic resistances and electronic nematicity, in which we are interested.[22,32]

ACKNOWLEDGMENTS

We acknowledge useful technical advice from Anthony T. Bollinger and Xi He. The research at Yale University was supported by the Gordon and Betty Moore Foundation's EPiQS Initiative through Grant No. GBMF9074.

AUTHOR DECLARATIONS

Conflict of Interest

The authors have no conflicts to disclose.

Author Contributions

Jin Zhao and Ivan Bespalov contributed equally to this work.

Jin Zhao: Formal analysis (lead); Investigation (equal); Visualization (lead); Writing – original draft (lead). **Ivan Bespalov**: Investigation (equal); Writing – review & editing (supporting). **Rongting Wu**: Methodology (lead); Validation (lead); Writing – review & editing (supporting). **Ivan Božović**: Conceptualization (lead); Funding acquisition (lead); Supervision (lead); Writing – review & editing (lead).

DATA AVAILABILITY

The data that support the findings of this study are available from the corresponding authors upon reasonable request.

REFERENCES

[1] V. L. Ginzburg and D. A. Kirzhnits, "On the superconductivity of electrons at the surface levels," Zh. Eksp. Teor. Fiz **46**, 397 (1964); Sov. Phys. JETP 19, 269 (1964).

[2] K. Ghosh, H. Rahaman, and P. Bhattacharyya, "Prediction and implementation of graphene and other two-dimensional material based superconductors: A review," IEEE Trans. Appl. Supercond. **30**(2), 7400109 (2020).

[3] G. Li, Y. Zhao, S. Zeng, M. Zulfiqar, and J. Ni, "Strain effect on the superconductivity in borophenes," J. Phys. Chem. C **122**(29), 16916 (2018).

[4] L. Yan, R. Ku, J. Zou, L. Zhou, J. Zhao, X. Jiang, and B.-T. Wang, "Prediction of superconductivity in bilayer borophenes," RSC Adv. **11**(63), 40220 (2021).

[5] Y. Mu, B.-T. Wang, S.-D. Li, and F. Ding, "A family of superconducting boron crystals made of stacked bilayer borophenes," Nanoscale **14**(27), 9754 (2022).

[6] M. Gao, Q.-Z. Li, X.-W. Yan, and J. Wang, "Prediction of phonon-mediated superconductivity in borophene," Phys. Rev. B **95**(2), 024505 (2017).

[7] Y. Zhao, S. Zeng, C. Lian, Z. Dai, S. Meng, and J. Ni, "Multigap anisotropic superconductivity in borophenes," Phys. Rev. B **98**(13), 134514 (2018).

[8] Z. Zhang, A. J. Mannix, Z. Hu, B. Kiraly, N. P. Guisinger, M. C. Hersam, and B. I. Yakobson, "Substrate-induced nanoscale undulations of borophene on silver," Nano Lett. **16**(10), 6622 (2016).

[9] R. Wu, I. K. Drozdov, S. Eltinge, P. Zahl, S. Ismail-Beigi, I. Božović, and A. Gozar, "Large-area single-crystal sheets of borophene on Cu(111) surfaces," Nat. Nanotechnol. **14**(1), 44 (2019).

[10] R. Wu, A. Gozar, and I. Božović, "Large-area borophene sheets on sacrificial Cu(111) films promoted by recrystallization from subsurface boron," npj Quantum Mater. **4**, 40 (2019).

[11] R. Wu, S. Eltinge, I. K. Drozdov, A. Gozar, P. Zahl, J. T. Sadowski, S. Ismail-Beigi, and I. Božović, "Micrometre-scale single-crystalline borophene on a square-lattice Cu(100) surface," Nat. Chem. **14**, 377 (2022).

[12] A. Srivastava, D. S. Dkhar, N. Singh, U. P. Azad, and P. Chandra, "Exploring the potential applications of engineered borophene in nanobiosensing and theranostics," Biosensors **13**(7), 740 (2023).

[13] M. Ou, X. Wang, L. Yu, C. Liu, W. Tao, X. Ji, and L. Mei, "The emergence and evolution of borophene," Adv. Sci. **8**(12), 2001801 (2021).

[14] C. Chen, H. Lv, P. Zhang, Z. Zhuo, Y. Wang, C. Ma, W. Li, X. Wang, B. Feng, P. Cheng, X. Wu, K. Wu, and L. Chen, "Synthesis of bilayer borophene," Nat. Chem. **14**(1), 25 (2022).

[15] E. Bauer, "Low energy electron microscopy," Rep. Prog. Phys. **57**, 895 (1994).

[16] J. B. Hannon and R. M. Tromp, "Low-energy electron microscopy of surface phase transitions," Annu. Rev. Mater. Res. **33**, 263 (2003).

[17] M. S. Altman, "Trends in low energy electron microscopy," J. Phys.: Condens. Matter **22**, 084017 (2010).

[18] J. C. Li, Y. Wang, and D. C. Ba, "Characterization of semiconductor surface conductivity by using microscopic four-point probe technique," Phys. Proc. **32**, 347 (2012).

[19] I. Miccoli, F. Edler, H. Pfnür, and C. Tegenkamp, "The 100th anniversary of the four-point probe technique: The role of probe geometries in isotropic and anisotropic systems," J. Phys.: Condens. Matter **27**(22), 223201 (2015).

[20] I. Shiraki, T. Nagao, S. Hasegawa, C. L. Petersen, P. Bøggild, T. M. Hansen, and F. Hansen, "Micro-four-point probes in a UHV scanning electron microscope for in-situ surface-conductivity measurements," Surf. Rev. Lett. **7**, 533 (2000).

[21] I. Shiraki, F. Tanabe, R. Hobara, T. Nagao, and S. Hasegawa, "Independently driven four-tip probes for conductivity measurements in ultrahigh vacuum," Surf. Sci. **493**(1–3), 633 (2001).

[22] J. Wu, A. T. Bollinger, X. He, and I. Božović, "Spontaneous breaking of rotational symmetry in copper oxide superconductors," Nature **547**(7664), 432 (2017).

[23] D. Zhao and D. Haneman, "LEED structures on Si(111) surfaces quenched from elevated-temperature cleavages," Surf. Sci. **418**, 132 (1998).

[24] R. M. Feenstra and M. A. Lutz, "Kinetics of the Si(111)$_2$ × 1 → 5 × 5 and 7 × 7 transformation studied by scanning tunneling microscopy," Surf. Sci. **243**, 151 (1991).

[25] P. Hofmann and J. W. Wells, "Surface-sensitive conductance measurements," J. Phys.: Condens. Matter **21**(1), 013003 (2008).

[26] R. Losio, K. N. Altmann, and F. J. Himpsel, "Continuous transition from two- to one-dimensional states in Si(111)-(5 × 2)-Au," Phys. Rev. Lett. **85**(4), 808 (2000).

[27] J. E. Demuth, B. N. J. Persson, and A. J. Schell-Sorokin, "Temperature-dependent surface states and transitions of Si(111)-7 × 7," Phys. Rev. Lett. **51**(24), 2214 (1983).

[28] R. Schillinger, C. Bromberger, H. J. Jänsch, H. Kleine, O. Kühlert, C. Weindel, and D. Fick, "Metallic Si(111)-(7 × 7)-reconstruction: A surface close to a Mott–Hubbard metal-insulator transition," Phys. Rev. B **72**(11), 115314 (2005).

[29] A. B. Odobescu, A. A. Maizlakh, and S. V. Zaitsev-Zotov, "Electron correlation effects in transport and tunneling spectroscopy of the Si(111)-7 × 7 surface," Phys. Rev. B **92**(16), 165313 (2015).

[30] M. Smeu, H. Guo, W. Ji, and R. A. Wolkow, "Electronic properties of Si(111)-7 × 7 and related reconstructions: Density functional theory calculations," Phys. Rev. B **85**(19), 195315 (2012).

[31] S. Modesti, P. M. Sheverdyaeva, P. Moras, C. Carbone, M. Caputo, M. Marsi, E. Tosatti, and G. Profeta, "Low-temperature insulating phase of the Si(111)-7 × 7 surface," Phys. Rev. B **102**(3), 035429 (2020).

[32] J. Wårdh, M. Granath, J. Wu, A. T. Bollinger, X. He, and I. Božović, "Colossal transverse magnetoresistance due to nematic superconducting phase fluctuations in a copper oxide," PNAS Nexus **2**(8), pgad255 (2023).